J|A|C|S
ARTICLES
Published on Web 03/12/2002

Dynamics of Alkane Hydroxylation at the Non-Heme Diiron Center in Methane Monooxygenase

Victor Guallar, Benjamin F. Gherman, William H. Miller,* Stephen J. Lippard,* and Richard A. Friesner*

Contribution from the Departments of Chemistry, University of California, Berkeley, California 94720, Massachusetts Institute of Technology, Cambridge, Massachusetts 02139, and Columbia University, New York 10027

Received July 30, 2001

Abstract: Semiclassical molecular dynamics simulations have been combined with quantum chemistry calculations to provide detailed modeling of the methane and ethane hydroxylation reactions catalyzed by the hydroxylase enzymes of the soluble methane monooxygenase system. The experimental distribution of enantiomeric alcohols in the reaction of ethanes made chiral by the use of hydrogen isotopes is quantitatively reproduced and explained. The reaction dynamics involve a mixture of concerted and bound radical trajectories, and we characterize each of these reactive channels in detail. Diffusion of the bound radical intermediate at the active site core determines the global rate constant. The results also provide a qualitative rationale for the lack of ring-opened products derived from certain radical clock substrate probes and for the relative rate constants and kinetic isotope effects exhibited by a variety of substrates.

The soluble methane monooxygenase (sMMO) has been the subject of intense theoretical and experimental investigation for the past decade.[1] The hydroxylase component (MMOH) of sMMO converts methane and dioxygen into methanol at room temperature by means of a carboxylate-bridged diiron center. Several intermediate states of the catalytic cycle have been characterized in previous experimental work. Intermediate Q, which contains a putative di(μ-oxo)diiron(IV) core, has been identified as the active species in the methane hydroxylation step.

In previous work, we performed detailed theoretical studies of intermediates in the MMOH catalytic cycle by using ab initio quantum chemical methods and a large ($\sim$100 atom) model for the enzyme active site.[2,3] In particular, we proposed a model for Q in which a water molecule remains coordinated to one of the iron atoms, as opposed to alternative models in the literature in which a shifting carboxylate group displaces this water molecule. We then used this model of Q to carry out a preliminary investigation of the methane hydroxylation reaction, catalyzed by MMOH, and found evidence for contributions to the dynamics from both concerted and bound radical pathways. This analysis[3] relied upon a heuristic scrutiny of the potential surface, however, rather than an actual computation of the reaction dynamics. Clearly, such a computation is necessary to produce a quantitative characterization of the reaction. Moreover, an understanding of the reaction dynamics has the potential to supply a rigorous understanding of previously observed experimental data that have thus far been difficult to reconcile with any single description of the C−H bond activation pathway. The results of studies with radical clock substrate probes[4−7] and with chiral ethane,[8,9] both of which have suggested radical lifetimes that are too short to be consistent solely with a discrete radical intermediate, are included.

Computer simulations of proton and hydrogen atom transfer reactions are particularly difficult because the description of proton motion requires the inclusion of quantum mechanical effects such as zero point energy, tunneling, and interference phenomena. Despite these difficulties, a number of mixed quantum-classical methods have been applied to simulate proton transfer.[10−13] In recent work,[14,15] rigorous semiclassical methods were developed to simulate ultrafast proton-transfer dynamics. These methods could reproduce exact quantum dynamics simulations and validate simpler semiclassical methods capable of obtaining picosecond time scale dynamics.

(1) Merkx, M.; Kopp, D. A.; Sazinsky, M. H.; Blazyk, J. L.; Müller, J.; Lippard, S. J. *Angew. Chem., Int. Ed.* **2001**, *40*, 4000−4025.
(2) Dunietz, B. D.; Beachy, M. D.; Cao, V.; Whittington, D. A.; Lippard, S. J.; Friesner, R. A. *J. Am. Chem. Soc.* **2000**, *122*, 2828−2839.
(3) Gherman, B. F.; Dunietz, B. D.; Whittington, D. A.; Lippard, S. J.; Friesner, R. A. *J. Am. Chem. Soc.* **2001**, *123*, 3836−3837.
(4) Ruzicka, F.; Huang, D.-S.; Donnelly, M. I.; Frey, P. A. *Biochemistry* **1989**, *29*, 1696−1700.
(5) Liu, K. E.; Johnson, C. C.; Newcomb, M.; Lippard, S. J. *J. Am. Chem. Soc.* **1993**, *115*, 939−947.
(6) Toy, P. H.; Newcomb, M.; Hollenberg, P. F. *J. Am. Chem. Soc.* **1998**, *120*, 7719−7729.
(7) Valentine, A. M.; LeTadic-Biadatti, M.-H.; Toy, P. H.; Newcomb, M.; Lippard, S. J. *J. Biol. Chem.* **1999**, *274*, 10771−10776.
(8) Priestley, N. D.; Floss, H. G.; Froland, W. A.; Lipscomb, J. D.; Williams, P. G.; Morimoto, H. *J. Am. Chem. Soc.* **1992**, *114*, 7561−7562.
(9) Valentine, A. M.; Wilkinson, B.; Liu, K. E.; Komar-Panicucci, S.; Priestly, N. D.; Williams, P. G.; Morimoto, H.; Floss, H. G.; Lippard, S. J. *J. Am. Chem. Soc.* **1997**, *119*, 1818−1827.
(10) Truhlar, D. G.; Liu, Y. P.; Schenter, G. K.; Garrett, B. C. *J. Phys. Chem.* **1994**, *98*, 8396.
(11) Koper, M. T. M.; Voth, G. A. *Chem. Phys. Lett.* **1998**, *282*, 100−106.
(12) Borgis, D. T. G.; Azzuoz, H. *J. Phys. Chem.* **1992**, *96*, 3188.
(13) Aqvist, J.; Warshel, A. *Chem. Rev.* **1993**, *93*, 2523.
(14) Guallar, V.; Batista, V.; Miller, W. H. *J. Chem. Phys.* **1999**, *110*, 9922−9936.
(15) Guallar, V.; Batista, V.; Miller, W. H. *J. Chem. Phys.* **2000**, *113*, 9510.

In the present paper, we address the hydroxylation dynamics in MMOH. In the first step we construct, through quantum chemical calculations, a reduced (four) dimensional surface on which the reaction takes place adiabatically, with minimization of the remaining enzyme coordinates. We then employ semiclassical trajectory computations to determine reaction rates and branching ratios. We focus our attention on the reaction of ethane with intermediate Q of MMOH, with the goal of providing a detailed explanation of the experimental results for the hydroxylation of the R and S isomers of CH_3CHDT.[8,9] Experiments with these substrates reveal a 2:1 ratio of retention to inversion in the chiral ethanol products, despite the fact that the ethyl radical racemizes in the gas phase in less than 100 fs. Our calculated product distribution is in excellent agreement with these experimental results. In addition, the calculations provide a comprehensive, microscopic picture of key features of the potential energy surface and how the substrate traverses the various dynamical pathways. The semiclassical formalism allows tunneling and zero point effects to be treated in an approximate fashion. The results should be applicable to other MMOH substrates.

The paper is organized in the following manner. In the Description of Calculations section we discuss the quantum chemical model of the enzyme active site, overall approach to the calculations, and details of the quantum chemical and semiclassical dynamics methodologies. In the Results we present the potential surface and the semiclassical dynamics of the hydroxylation reaction. In the Discussion section we analyze the results to obtain physical insight from the calculations, and the Conclusion summarizes what we have learned and briefly discusses future directions.

Description of Calculations

A. Overall Strategy. The model used for intermediate Q and its interaction with methane was described previously.[2,3] It contains on the order of 100 atoms and provides accurate structures and energies for the components of the MMOH catalytic cycle. The generation of a transition state in which ethane, rather than methane, is the substrate is straightforward, given our previous results for methane, and is discussed further below.

Our first objective in this work is to generate a potential energy surface for the ethane reaction that can be used to study the reaction dynamics in detail. For this purpose, it is sufficient that the relative energies of points on the surface are in reasonable agreement with accurate quantum chemical results. Generation of the potential surface over four degrees of freedom is a challenging task, given the size of the model we have chosen to study. Consequently, we constructed the surface using a DZP basis in the core region rather than the more accurate TZ2P basis employed in previous work to obtain energy differences between structures that are chemically quite different, such as the different intermediates in the catalytic cycle. We checked this approximation by computing energies at a small number of points using the larger basis set and examining the energy differences. The results demonstrate that basis set effects on the potential surface are relatively small and can reasonably be neglected in the present study.[16]

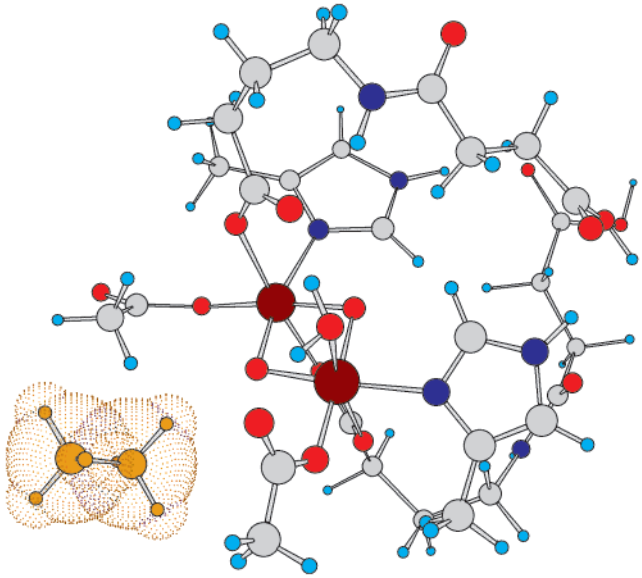

Figure 1. Active site model. The ethane approaching the active site is depicted with van der Waals dotted surface. The two irons are described with LACVP**, the ethane, water ligand, oxygens within three bond distances from the irons (and carbons linking them), and histidine nitrogen next to the iron are described with 6-31g**, and the remaining atoms are described using 6-31g.

Once the potential energy surface was generated, we investigated the dynamics by means of semiclassical trajectory calculations. We used methods that were previously described and tested for accuracy in a number of model systems. Although these computations cannot be considered to be at a benchmark level, they include important quantum effects, such as zero point energies and tunneling, in a plausible fashion and hence can be expected to provide semiquantitative accuracy. Our comparisons with the experimental data suggested that we achieved a reasonable level of accuracy, although further calculations for additional substrates and experimental observables, such as kinetic isotope effects, are necessary to validate fully the protocols that were employed.

B. Electronic Calculations, Active Site Model. All electronic structure calculations were carried out with the Jaguar v4.1[16] suite of ab initio quantum chemistry programs, using unrestricted DFT (UDFT) with the B3LYP functional. The active site model is represented in Figure 1. Computational methods and structural modeling strategies have been extensively described elsewhere. The basis set used is also summarized in Figure 1. The main atoms involved in the reaction dynamics were modeled with 6-31g** and, for the iron atoms, LACVP**. The remaining atoms were described with 6-31g. As already stated, the accuracy of the basis set was checked with TPZ optimization for several structures.

C. Trajectories. Classical trajectories were integrated according to a standard fourth-order Runge−Kutta algorithm, with a 0.096 fs integration step. All forces necessary for integrating the equations of motion were calculated by using finite

(16) The energy difference between two constrained radical intermediate minimums (different C−O distance constrained) was 2.15/1.95 kcal/mol with DZP and TZ2P, respectively. Reoptimization of both transition states results in an energy barrier of 4.01/3.82 kcal/mol for the rotation and 11.5/10.86 kcal/mol for the proton transfer (from the intermediate bound radical) for DZP and TZ2P, respectively. All quantum chemistry calculations were carried out with Jaguar 4.1, Schrödinger, Inc., Portland, OR, 1991−2000.

difference expressions. Initial conditions for the semiclassical trajectories were sampled using the Wigner function for the Boltzmannized operator with the harmonic normal mode approximation, $\rho^{W}(q,p)$, eq 1, where q and p are the initial coordinate and momentum for each degree of freedom. Making

$$\rho^{W}(q,p) = \int d\Delta q e^{-ip\Delta q}\left\langle q + \frac{\Delta q}{2}\middle| e^{-\beta\hat{H}} \middle| q - \frac{\Delta q}{2}\right\rangle \qquad (1)$$

use of the matrix elements in eq 2, the integration is reduced to

$$\langle q_i|e^{-\beta\hat{H}}|q_i'\rangle = \left[\frac{m_i\omega_i}{2\pi\hbar\sinh(2u_i)}\right]^{1/2} \times \exp\left\{-\frac{m_i\omega_i}{2\hbar\sinh(2u_i)}[(q_i^2 + q'^2_i)\cosh(2u_i) - 2q_iq_i']\right\} \qquad (2)$$

a Gaussian type integral, obtaining $\rho^{W}(q,p)$, eq 3. In this equation, we denote $u_i = \hbar\beta w_i/2$, introducing a temperature

$$\rho^{W}(q_ip_i) = \frac{1}{2\sinh(u_i)}\left\{\frac{\tanh(u_i)}{\pi\hbar}\exp\left[\frac{2\tanh(u_i)}{\hbar w_i}\left(\frac{p_i^2}{2m_i} + \frac{1}{2}m_iw_i^2q_i^2\right)\right]\right\} \qquad (3)$$

factor in a straightforward sampling procedure.

D. Tunneling Description. Use of the Wigner function in the initial sampling incorporates some quantum effects. Specifically, the quantum behavior is well described for short time, $t < \beta\hbar$; the longer time dynamics derive strictly from classical mechanics. Tunneling corrections were therefore improved through a WKB treatment of sudden proton transfer at classical turning points. The probability of tunneling at each classical turning point is given by eq 4, where m is the mass of the tunneling coordinate, $E(r)$ is the potential energy along the

$$P_t = \int_{r_i}^{r_f} \exp(-2)\sqrt{2m(E(r) - E_{r_i})}\,dr \qquad (4)$$

sudden tunneling path, and $E(r_i)$ is the initial energy at the turning point. The WKB method employed, based on previous work,[17,18] is very simple and only slightly more expensive than a totally classical propagation. At each classical turning point along any q coordinate, where tunneling might be important, a sudden transfer path with all the degrees of freedom but frozen in q is projected. If the sudden transfer path finds a classically accessible exit point, that is, $E(r_f) = E(r_i)$, then a positive probability, P_t, can be defined and the transfer accepted if $P_t/r > 1$, r being a [0:1] random number. If the transfer is accepted, the trajectory continues at $q = r_f$ after the tunneling event. Recently[15] this method gave excellent results when compared with more rigorous semiclassical calculations in a proton-transfer reaction.

Results

A. Potential Surface. The reaction dynamics of the ethane hydroxylation were simulated by construction of a reduced dimensionality electronic potential energy surface (PES). The PES describes the hydrogen atom dynamics in terms of the three main coordinates as described in Figure 2. In the figure, R_1 is the O−H/C−H distance after/before the transition state in the

(17) Tully, J. C.; Preston, R. K. *J. Chem. Phys.* **1971**, *55*, 562−572.
(18) Makri, N.; Miller, W. H. *J. Chem. Phys.* **1989**, *91*, 4026.

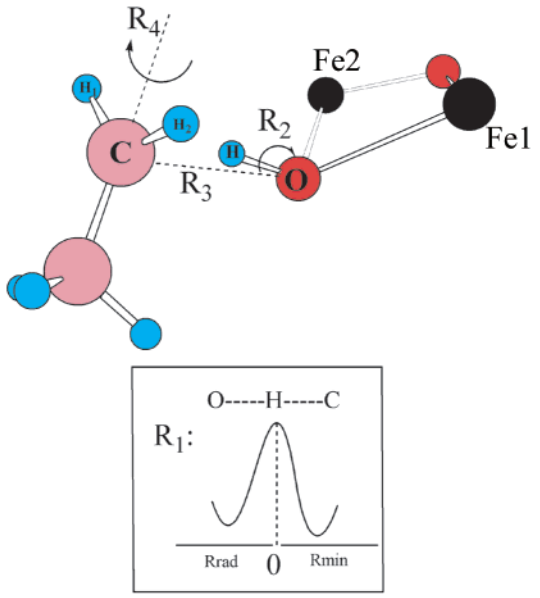

Figure 2. Reaction coordinates for the reduced potential surface employed to model the ethane hydroxylation dynamics.

Table 1. Energy and Distance Summary[a]

	methane	ethane
hydrogen transfer barrier	16	12.5
$E_{\text{br intermediate}} - E_{\text{reactant}}$	5	1
H rotation barrier	3.9	4.01
reactant C−O distance	3.73	3.77
br intermediate C−O distance	3.1	3.06

[a] Energies are in kcal/mol, and distances are in angstroms; br = bound radical.

H atom transfer, R_2 is the C···H−O angle, and R_3 is the C···O distance. The C−C bond rotation that could exchange H_1 and H_2 in a chiral ethyl radical and afford racemized products from chiral ethane is defined as R_4 (Figure 2). The full dimensional PES was then adiabatically reduced to these main reaction coordinates through geometry optimization of all the remaining degrees of freedom, with an overall small displacement in the reaction, for several representative configurations of R_1−R_4. The active site model enzyme (Figure 1) is the same as previously described,[2] consisting of 97 atoms, for a total of 105 atoms in the system when modeling ethane as a substrate.

The main energetic parameters involved in the hydroxylation reaction and a comparison with results for the methane−MMOH[3] system are summarized in Table 1. The energy barrier for hydrogen atom transfer along the R_1 coordinate (Figure 2) is 12.5 kcal/mol, significantly smaller than the one for the MMOH hydroxylation of methane, 16 kcal/mol. The latter value is slightly smaller than that of 18 kcal/mol, uncorrected for zero point effects, reported previously.[3] The minor difference in barriers can be a consequence of (i) the different basis set, (ii) the single point recalculation in the previous work compared with the optimization methodology applied here, and/or (iii) the localization of a van der Waals reactant structure in our more detailed exploration of the reaction dynamics potential energy surface. Transfer of the hydrogen atom affords a bound radical intermediate (Rrad in Figure 2), in which the C−O distance is 3.1 Å for methane−MMOH and 3.06 Å for ethane−MMOH. The energies of this intermediate relative to the reactant minimum for $R-CH_3$ + MMOH (R = H for methane and CH_3

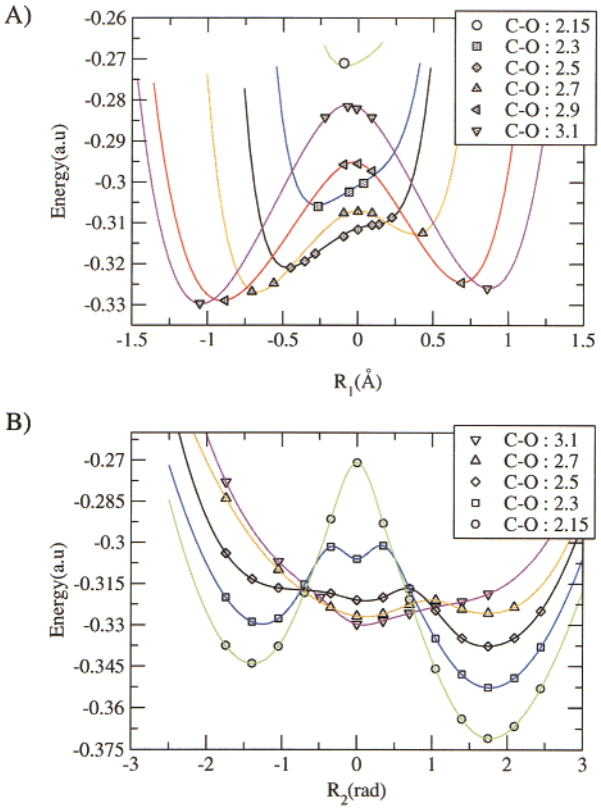

Figure 3. Panel A: Ab initio results and interpolated energy profile along R_1 at various different R_3 values, constructed in terms of two Morse potentials associated with the equilibrium positions of the donor and acceptor configurations. Panel B: Ab initio results and interpolated energy profile along R_2 at various different C−O distance values, R_3, built by using a two-dimensional spline procedure.

for ethane) are 5 and 1 kcal/mol, respectively. For the rotation along R_2 (Figure 2), both methane and ethane systems present very similar barriers of 3.90 and 4.01 kcal/mol, respectively.

These energy parameters are strongly coupled with R_3, the C−O distance, and a more detailed exploration of the potential within this coordinate is necessary to build an accurate PES. Through our dynamics, R_3 is built as a global, mass-weighted reorganization coordinate, including all the substrate displacements for each C−O distance. We set R_3 to be zero at C−O = 2.5 Å, introducing negative R_3 values for those C−O distances <2.5 Å and positive R_3 values for C−O distances >2.5 Å.

Figure 3A shows the energy profile along R_1 at various different R_3 values. These energy profiles along the R_1 coordinate are constructed in terms of two Morse potentials associated with the equilibrium positions of the donor and acceptor configurations as a function of R_3, coupled by adjusting the energy barrier to the UDFT TS energy for each particular R_3 constrained geometry. A negative R_1 value indicates that the H atom has transferred from the alkane reactant and is in the bound radical intermediate well. Figure 3A clearly shows that the H atom-transfer energy barrier decreases as R_3 diminishes to 2.5 Å, that is, when the distance between the H atom donor (ethane) and the H atom acceptor (O−Fe) decreases. In the transition state (TS) for proton transfer, which has a barrier height of 12.5 kcal/mol, the C−O distance is 2.5 Å (R3 = 0). The reaction is exothermic for practically all the configurations where the barrier is small enough to allow the transfer to take place. The exothermic character of the reaction decreases as R_3 increases. The reaction becomes endothermic with very large barriers for those C−O distances close to the absolute minimum of 3.77 Å. These results indicate that the promoting mode for hydrogen atom transfer is the approach of the substrate to the reactive oxygen nucleus at the active site.

After the hydrogen is transferred to the oxygen atom of intermediate Q in MMOH, forming an O−H bond, the principal character of the substrate, whatever its precise location, is that of a bound radical. Mulliken population analysis indicates an unpaired electron located on the donor carbon atom (C in Figure 2) and a total charge of zero for the ethyl intermediate after the H atom transfer. At this point, ethanol formation can proceed from the radical intermediate minimum, or from any bound radical intermediate at different R_3 values, by rotation of the hydrogen of the O−H group out of the Fe−O−Fe plane. Figure 3B shows the energy profile along R_2 at various different R_3 values. The energy values for $R_2 = 0$ in Figure 3B correspond to the bound radical intermediate minima in Figure 3A. These energy profiles along R_2 and R_3 were built by using a two-dimensional spline interpolation procedure. Positive values for R_2 indicate rotation upward from the C···H···O collinear distance, as shown in Figure 2, whereas R_2 negative values indicate rotation in the opposite direction. These two different rotations define two possible channels for the hydroxylation reaction. The first notable feature in Figure 3B is the large exothermicity of the rotation profile for very short C−O distances (R3 < 0), the real driving force for the overall hydroxylation reaction. After rotation the carbon atom will rapidly and spontaneously move toward the O atom to form alcohol bound to the diiron core. As stated previously,[2] once the C−O bond is formed, the resulting ethanol moiety will spontaneously leave the diiron core in an energy minimization protocol, indicating the absence of a barrier for this process. The energy parameters involved in this rotation are almost identical to the one previously obtained for the methane−MMOH hydroxylation reaction, indicating a similar mechanism in the overall hydroxylation reaction dynamics for both substrates.

Figure 4 displays the contour and the 3-D potential surface plot for the R_1 and R_2 coordinates at three different R_3 values. In panel A, for a C−O distance of 2.15 Å, we can clearly distinguish the two rotation channels leading to ethanol, with no significant accessible regions along the R1 coordinate. In panels B and C we observe the evolution of the potential surface as the C−O distance increases, leading to two well-defined minima for the H atom transfer coordinate, R_1.

Aside from the R_1−R_3 coordinates, describing the main aspects of the hydrogen transfer and rotation, we have included an additional degree of freedom (R_4) describing rotation around the C−C bond of the ethyl radical. Rotation about R_4 can interchange hydrogen atoms H_1 and H_2 of the ethyl radical, leading to inversion of configuration in chiral ethane, that is, when D and T replace H_1 and H_2.[8,9] Figure 5 shows the energy profile along R_4 at various different R_3 values. These energy profiles were constructed by periodically cloning two harmonic wells associated with the multiple equilibrium positions for the rotation process, $\pi/2 + n\pi$, where n is an integer, coupled by adjusting the energy barrier to the UDFT TS rotational transition states energy for each particular value of R_3. As indicated in Figure 5, the rotation is forbidden for short C−O distances as a result of steric factors owing to the proximity of either H_1 or

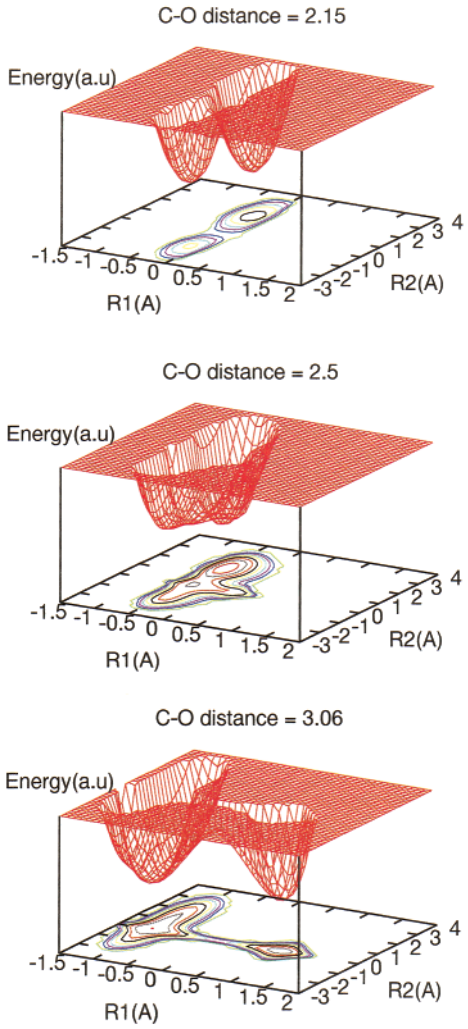

Figure 4. Contour and 3-D potential surface plot for the R_1 and R_2 coordinates at three different C−O distances.

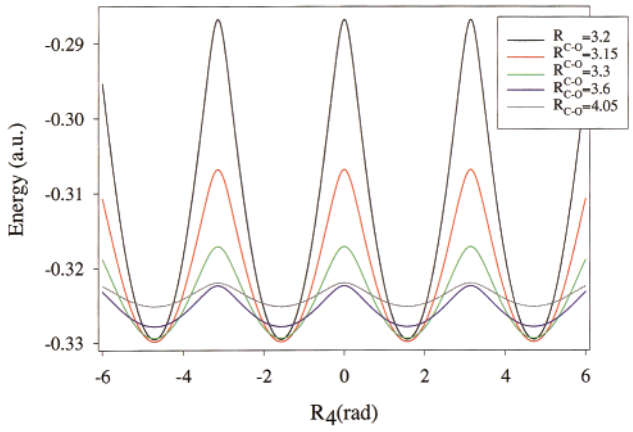

Figure 5. Energy profile along R_4 at various different R_3 values.

H_2 to the already transferred hydrogen atom. The barrier for rotation along R_4 is 4.06 kcal/mol, with a 3.7 Å value for the C−O distance at the TS. This longer C−O distance in the TS (the C−O distance in the minimum is 3.06 Å) introduces an effective barrier for large C−O distances of ∼1.5 kcal/mol. This result is very important since rotation of the ethyl radical in the gas phase behaves almost like a free rotor, with a period for an inversion of ∼200 fs at room temperature. Our calculations thus demonstrate how the enzyme environment retards the gas-phase free rotation and controls it by energy redistribution. The possibility that stereoelectronic effects of this kind occur for MMOH hydroxylation reactions was previously considered in a discussion of the results with radical clock substrate probes, but with no clear picture of how they might arise.[5]

The intermediate in a methane hydroxylation reaction has more hydrogen rotation possibilities than in the ethane case. The methane radical has three equivalent hydrogen atoms able to interchange their positions by rotation, whereas the ethyl radical has only two. We estimated the methyl radical rotation barrier, observing very similar results of ∼4 kcal/mol, for each of the possible rotations. Following the behavior described in Figure 5, each rotation barrier for the methyl radical increases considerably when the C−O distance diminishes.

B. Dynamics for the Ethane−MMOH Hydroxylation Reaction. The main purpose of our simulation is to sample the reaction flux following the hydrogen atom transfer step. In particular, we were interested in measuring the relative contributions of the concerted versus recoil/rebound reaction pathways[1] as well as the percent inversion versus retention in the product alcohol for chiral ethane as the substrate. To obtain the reaction flux over possible pathways emanating from the transition state, we sampled semiclassical trajectories in the region $R_1 = 0$. The remaining positions and momenta were sampled via the Wigner distribution described in the Description of Calculations section. To reproduce the experimental conditions, the temperature for the Boltzmannized sampling was set to 318 K. The momentum in R_1 was initially chosen to have negative values to optimize the reactive flux and to obtain minimum initial recrossing. When modeling the dynamics for R_4, we have reproduced the chirality of the reactant ethane by defining deuterium and tritium as the hydrogen isotopes for H_1 and H_2, with an effective moment of inertia of $\sim 5 * m_H * r^2$, where $m_H = 1836$ au and $r_0 = 1.72$ au.

Figure 6 plots three representative trajectories obtained by running semiclassical trajectories on the PES described in the previous section. As previously introduced, positive values of R_1 indicate the hydrogen atom being in the reactant well, whereas for negative values the system is in the bound radical intermediate region. The parameter R_2 correlates directly with the C−O−H angle. We assume that the product (ethanol) is obtained whenever R_3 is smaller than −2.4, which is the value corresponding to a C−O distance smaller than 2.15 Å. The R_4 parameter, initially sampled around $-\pi/2$, has minimum values at each $\pm\pi/2 + n*\pi$, where n is an integer.

The converged results for the concerted versus recoil/rebound mechanisms and the calculated percent inversion/retention of configuration are shown in Table 2. The results, which converged with 10 000 trajectories, reveal that 16.5% of the hydroxylation reaction follows a purely concerted path, forming ethanol without evolving through the radical intermediate minimum. This amount of concerted reaction product becomes 12.5% when WKB tunneling corrections are switched off. The remaining trajectories, which evolve through recoil to afford a bound radical intermediate, define a radical mean lifetime. This quantity is calculated as the average radical intermediate lifetime, for lifetimes greater than 20 fs, eliminating fast recrossing events in the radical well that would considerably decrease this mean value. The converged results indicate a radical mean lifetime of 320 and 400 fs for WKB and classical propagation,

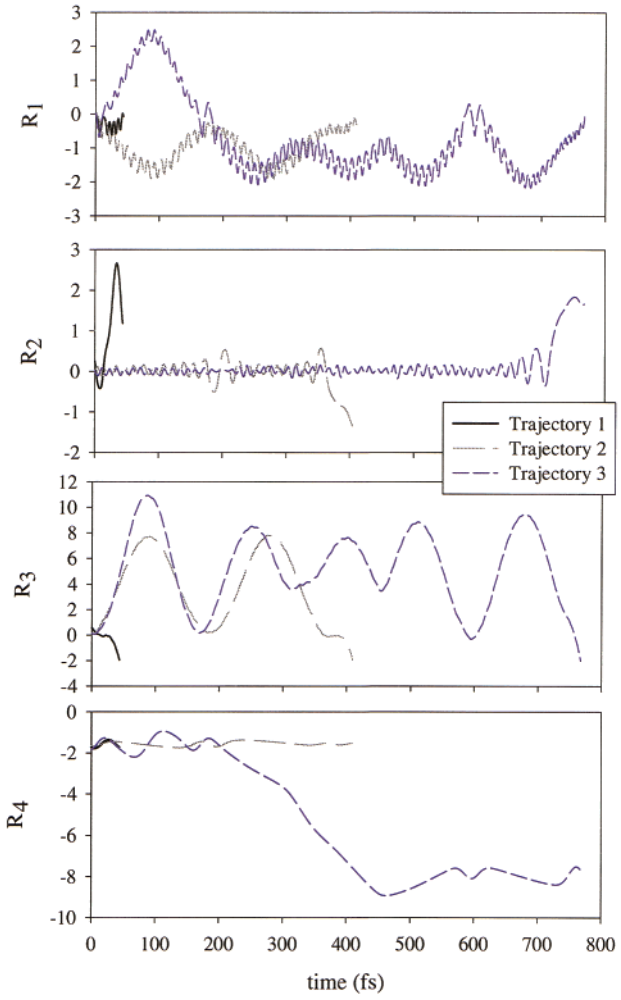

Figure 6. Three representative semiclassical trajectories. Each panel shows the evolution of one of the main four reduced coordinates R_1-R_4.

Table 2. Converged Dynamics Results for the Radical Mean Lifetime, and Percentage of Reactions Traversing Converted versus Rebound Mechanism[a]

	ethane no tunnel/WKB
rad lifetime (fs)	400/320
concerted channel (%)	12.4/16.5
% retention ($R4(0) = -1.57$)	84/85
% retention ($R4(0) = -1.67$)	79/79
% retention ($R4(0) = -1.77$)	68/69

[a] The net configuration retention is also tabulated. Results were converged after 10 000 trajectories.

respectively. Clearly the radical, as discussed below, is bound and not a discrete species.

To simulate the amount of configuration retention, we initially centered R_4 around $-\pi/2$, that is, sampling all the rotamers in one configuration. The amount of retention, shown in Table 2, is quite sensitive to the initial position of the center of the sampling function for R_4. The transition state structure displays an initial deviation for H_1 and H_2 from the planar sp^2 geometry of the bound radical intermediate minimum. More precisely, a dihedral angle of ~15° (0.26 rad) between unrotated and rotated planes should result in an initial increase in energy. Both hydrogen atoms H_1 and H_2 in the TS structure are displaced backward from the planar geometry of the energy minimum. It is therefore not obvious how to project this initial deviation into the R_4 parameter, as required for a reduced dimensionality analysis. Table 2 indicates the results for the percentage of configuration retention at three different values for the center in the R_4 initial sampling, −1.57 (the radical intermediate minimum), −1.77 (an initial deviation of 0.2 rad), and −1.67 (an intermediate value). Rebound of the radical to form a C−O bond affords the final product methanol.

Discussion

The first obstacle in understanding the hydroxylation reaction dynamics is the hydrogen atom transfer barrier. This step, involving a 12.5 kcal/mol activation energy, a priori should be the rate-limiting step for the overall reaction. Our calculations reveal that ethane requires almost 4 kcal/mol less energy than that of the methane to reach this state. This energy stabilization factor is conserved throughout the radical dynamics pathway for the ethane, as compared to the methane, energy profile. The origin of this difference is the inductive effect of the methyl group in the ethyl radical. Radicals are intrinsically electron-deficient species, and methyl (in the ethyl radical) better serves to donate electrons than does a hydrogen atom (in the methyl radical), stabilizing the radical center. Ab initio results demonstrate that tertiary radicals are more stable than secondary and primary radicals by 5 and 3 kcal/mol, respectively.[19] Small radicals have displayed the same qualitative energy behavior in hydrogen-abstraction reactions in methane and ethane.[20,21] The difference is also reflected in the relative C−H bond energies of 105 ± 0.09 and 101.19 ± 0.09 kcal/mol, respectively, for methane and ethane.[22]

The barrier for rotation of the H atom in the −OH moiety, 4 kcal/mol, is large and implies that this rotation should proceed on the picosecond time scale. This energy is considerably less than that required to achieve the preceding hydrogen atom transfer step, however, and may be redistributed quickly toward rotation along the R_2 coordinate. The dynamics and trajectory analysis describes 16% of the reaction following a concerted pathway, where the system has enough energy, or can rapidly redistribute the energy, to rotate immediately after the transition state in the hydrogen atom transfer coordinate. Trajectory 1 in Figure 6 describes this concerted pathway. A close examination of the trajectory indicates that the system spends 25 fs in the transition state region, from $t = 5$ fs to $t = 30$ fs at $R_3 \approx 0$. When R_2 approaches the rotation barrier at 20 fs, there is energy transfer from R_1 and R_4, as observed in the weakness of its amplitudes, leading to a rotation toward positive R_2 values, the up-channel. Obviously, for this 16% contribution of concerted reaction, there is total retention since there is not enough time or energy to overcome the barrier to rotation along R_4.

The concerted path is significantly altered when tunneling contributions are added as a sudden H atom transfer path. We see an increase in the fraction of reactants following the concerted channel by almost $^1/_3$, indicating the importance of tunneling effects for an accurate description of the reaction dynamics. This large quantum effect agrees with the experimentally measured kinetic isotope effects; for example, k_H/k_D is 3.8 for hydroxylation of $R-CH_3CHTD$.[9]

(19) Marsi, I.; Viskolcz, B.; Seres, L. *J. Phys. Chem. A* **2000**, *104*, 4497−4504.
(20) Xu, Z.-F. *J. Phys. Chem. A* **1999**, *103*, 4910−4917.
(21) Marshall, P. *J. Phys. Chem. A* **1999**, *103*, 4560−4563.
(22) Berkowitz, J.; Ellison, G. B.; Gutman, D. P. *J. Phys. Chem. A* **1994**, *98*, 2744.

Besides the contribution from the concerted pathway, trajectories 2 and 3 summarize the dominant mechanism of the reaction. The dynamics reveal that most of the reactants follow the bound radical recoil/rebound pathway. Configurations with enough energy to reach the transition state in R_1 will typically execute many full vibrational periods in R_3, in both the reactant and the intermediate wells. Trajectory 3 requires one vibrational period in the reactant well and four in the intermediate well until the energy is effectively redistributed from R_1 to R_2. Trajectory 2, instead, needs only two periods in R_3, and we observe energy flow from both R_1 and R_4 to R_2. Trajectories 2 and 3 react within a picosecond after they reach the transition state in R_1. When integrating the amount of product formed with time, however, 4 ps are required for a complete reaction, with a constant interconversion between the bound radical and the reactant. We expect, therefore, that it is not hydrogen atom transfer alone that controls the overall rate constant, but also the diffusion of the bound radical intermediate along R_3.

Our active site model study reveals that 80% of the product is obtained through the up rotation channel ($R_2 > 0$) and the remaining 20% through the down rotation channel ($R_2 < 0$). The dynamics thus require a thorough description of both reactive channels, a conclusion not immediately obvious from a standard exploration of the potential surface.

The radical intermediate exhibits a strongly bonded character, with a "harmonic" motion along R_3 having a period of ~200 fs. For half of this period the C−O distance is less than 3.0 Å, and the radical can be considered to be a "bound" species. One might therefore expect to observe no radical-derived ring-opened products from radical clock substrate probes such as *trans*-phenylmethylcyclopropane. Indeed, experimental observations with this and related substrates[5,7] agree with this expectation. Rotation along R_4, with a possible configuration inversion, inhibits the motion along R_3 since the R_4 rotation barrier increases at the shorter C−O distances. This behavior is clearly observed in trajectory 3, where during the rotation process in R_4, from $t = 250$ fs to $t = 450$ fs, R_3 (and therefore the C−O distance) executes shorter amplitudes in its vibrational motion. It is this aspect of the dynamics that increases the mean lifetime of the radical intermediate from its 200 fs period to the 300 fs (400 without tunneling contributions) as presented in Table 2. In particular, trajectory 3 describes a 2π rotation along R_4, resulting in retention of configuration.

For the methane reaction we would expect larger retention of the methyl bound radical intermediate, due to the multiple rotation of each of the three possible pairs of hydrogen atoms. Since there is no fourth isotope of hydrogen, however, it is not possible experimentally to test this prediction. For larger hydrocarbons such as propane or butane, experimental measurements of retention of configuration, and hence the relative importance of the concerted and bound radical channels, are feasible. Because of the retarded motion of the radical intermediate for heavier substrates, we expect an increase in the transition state mean lifetime for H atom transfer, since its reaction coordinate involves considerable substrate displacement, or recoil. This increase in TS lifetime should translate into a larger percentage of concerted pathway and a larger contribution of tunneling trajectories, since almost all the tunneling is done in the proximity of the TS.

Integrating the R_4 rotation coordinate along the time axis, we compute 69−84% of configuration retention, depending upon the initial energy in R_4, in good agreement with the observed experimental value of 72% for R-chiral ethane.[9] Experimental results for butane hydroxylation[9] report a slight increase of the retention of configuration, 76% as compared to 72% for the ethane substrate, as expected if the percentage of concerted pathway is larger, as just discussed above for propane.

Conclusions

The present theoretical analysis presents a unified view of the reaction dynamics of the key hydroxylation step in the reaction of the diiron center in the hydroxylase component of soluble methane monooxygenase with alkane substrates. By combining quantum mechanics and dynamics, the distribution of products in the reaction of ethane made chiral by use of hydrogen isotopes has been quantitatively explained. An oxygen atom of the di(μ-oxo)diiron(IV) intermediate Q in the MMOH reaction pathway abstracts a hydrogen atom from the terminal methyl group of the substrate, affording a bound radical intermediate that can traverse various reaction pathways leading to a mixture of concerted and radical trajectories. The results provide a qualitative rationale for the lack of ring-opened products in many of the radical clock substrate probes examined in the sMMO system. Some results with such kinds of probes cannot be adequately accounted for by this qualitative extension of the model, especially those in which more sterically crowded methyl groups or secondary alkanes are employed as substrates.[1] In addition, more detailed analyses, currently in progress, are required to explain the unusual kinetic isotope effects reported with deuterated substrates and to characterize propane's potential surface from which the qualitative dynamics were inferred.

The computational model and methods employed in this study represent an advance as compared to many previous efforts. In particular, the construction of a multidimensional potential energy surface for the enzyme, using a large model of the active site and adiabatic minimization at a significant number of points on the surface, was a necessity to explore the full complexity of the dynamics. Nevertheless, significant improvements can be envisioned in future work. In particular, QM/MM rather than QM methods can be used to define the potential energy surface, thus allowing the full protein environment to be treated quantitatively. It would also be desirable to incorporate other vibrational modes of the system into the dynamics model, for example, as harmonic oscillators. There are various quantum dynamics formalisms that enable computations to be carried out for such a model. The key step is to work out an efficient way of mapping the quantum chemical potential energy surface onto a model potential of a suitable form. Also, the treatment of quantum effects used here, while reasonable, could be improved by using better quantum dynamics algorithms. Although it is unclear how much such an improved treatment would affect the results of the present analysis, it would certainly be valuable to be able systematically to increase the level of accuracy of the methodology. More work also needs to be done in specifying the initial conditions to a greater degree of precision. Finally, the methods described here can be applied to the study of reactions mediated by other metal-containing enzymes that catalyze hydroxylation reactions, such as cytochrome P450, as well as more generally to all sorts of enzymatic reactions. Detailed studies of a wider range of enzyme-catalyzed hydroxy-

lation reactions might afford a more general understanding of how the active site core and protein environment tune the reaction specificity.

Acknowledgment. This work was supported by grants GM32134 (to S.J.L.) from the National Institute of General Medical Sciences and GM-40526 (to R.A.F.). Computing resources were provided by the MSCF at Pacific Northwest Laboratories, the National Energy Research Scientific Computing Center (NERSC), and the NPACI program supported by the NSF. V.G. gratefully acknowledges the Spanish Ministry of Education for a postdoctoral fellowship.

JA0167248